HHS Public Access

Author manuscript

Arch Biochem Biophys. Author manuscript; available in PMC 2017 December 15.

Published in final edited form as:

Arch Biochem Biophys. 2016 December 15; 612: 46–56. doi:10.1016/j.abb.2016.10.011.

Ligand Binding Phenomena that Pertain to the Metabolic Function of Renalase

Brett A. Beaupre[1], **Joseph V. Roman**[1], **Matthew R. Hoag**[1], **Kathleen M. Meneely**[2], **Nicholas R. Silvaggi**[1], **Audrey L. Lamb**[2], and **Graham R. Moran**[1,*]

[1]Department of Chemistry and Biochemistry, University of Wisconsin-Milwaukee, 3210 N. Cramer St, Milwaukee, Wisconsin 53211-3209.

[2]Molecular Biosciences, University of Kansas, 1200 Sunnyside Ave, Lawrence, KS 66049.

Abstract

Renalase catalyzes the oxidation of isomers of β-NAD(P)H that carry the hydride in the 2 or 6 positions of the nicotinamide base to form β-NAD(P)$^+$. This activity is thought to alleviate inhibition of multiple β-NAD(P)-dependent enzymes of primary and secondary metabolism by these isomers. Here we present evidence for a variety of ligand binding phenomena relevant to the function of renalase. We offer evidence of the potential for primary metabolism inhibition with structures of malate dehydrogenase and lactate dehydrogenase bound to the 6-dihydroNAD isomer. The previously observed preference of renalase from *Pseudomonas* for NAD-derived substrates over those derived from NADP is accounted for by the structure of the enzyme in complex with NADPH. We also show that nicotinamide nucleosides and mononucloetides reduced in the 2- and 6-positions are renalase substrates, but bind weakly. A seven-fold enhancement of acquisition (k_{red}/K_d) for 6-dihydronicotinamide riboside was observed for human renalase in the presence of ADP. However, generally the addition of complement ligands, ADP for mononucloetide or AMP for nucleoside substrates, did not enhance the reductive half-reaction. Non-substrate nicotinamide nucleosides or nucleotides bind weakly suggesting that only β-NADH and β-NADPH compete with dinucleotide substrates for access to the active site.

Introduction

Renalase is an FAD-dependent oxidase that catalytically oxidizes two isomeric forms of β-NAD(P)H to form β-NAD(P)$^+$ and H_2O_2 (Scheme 1). These isomers are presumed to occur when β-NAD(P)$^+$ is reduced non-specifically forming, in addition to the native β-NAD(P)H (4-dihydroNAD(P)), 2-dihydroNAD(P) (2DHNAD(P)) and 6-dihydroNAD(P) (6DHNAD(P)) [1, 2]. Both 2DHNAD and 6DHNAD have been shown to be highly inhibitory to specific primary metabolism dehydrogenases [2]. This suggests that renalase has an intracellular metabolic house-keeping function that alleviates metabolic suppression by these isomers. This proposal differs starkly from the consensus view that renalase is a mammalian serum borne protein that is associated with an array of aberrant physiological conditions. The enzyme was originally claimed to be a kidney-derived hormone that down-

*To whom correspondence should be addressed: Ph: (414) 940 0059, Fax: (414) 229 5530, moran@uwm.edu.

modulates vascular tone in animals by the oxidation of catecholamines[3–7] and then later to be a cytokine that ameliorates myocardial damage resulting from an ischemic event[8]. More recently it has been said to be a suppressor of pancreatic cancer and/or an exacerbatory factor for melanoma [4, 9–12]. Here we present the first structures of 6-DHNAD in complex with malate dehydrogenase and lactate dehydrogenase, confirming our assertion that β-NAD(P)H [dihydronicotinamide] isomers are detrimental to normal metabolic activity and reasserting the verified catalytic function of renalase. These structures show that 6DHNAD occupies the β-NADH-binding site occluding the association of the native nicotinamide substrate.

With a modest two-electron reduction potential of −320 mV, the potential for non-specific redox reactions of β-NAD(P)$^+$ that form toxic β-NAD(P)H isomers exists in all living systems. It is therefore reasonable to expect that an intracellular detoxification activity such renalase would be found in multiple kingdoms of life. However, homology searches based on the human renalase amino acid sequence return almost exclusively homologs from *animalia*. The structure of human renalase (isoform 1; HsRen) was solved in 2011 by the Aliverti group who noted that the renalase structural topology was common to numerous redox active flavoproteins [13]. In this structure the open active site was observed to have only a small number of conserved amino acids indicating that sequence alignments based on overall alignment scores (E-values) may not detect this motif and will not necessarily identify distant forms of renalase. We have recently characterized a renalase from a Pseudomonad (19% identity to Human)[14]. As part of this study we solved the crystal structures of this form of renalase (PpRen) in complex with β-NADH (PDB ID 4ZCC, 2.1 Å; a fascimile of the ES complex) and β-NAD$^+$ (PDB ID 4ZCD, 1.7 Å; the EP complex). These structures revealed that the *si* face of the FAD isoalloxazine is closely associated with the inner surface of the active site offering the *re* face for interaction with the substrate nicotinamide base. The few conserved residues that line the dihydronicotinamide-binding cavity are: PpRen H232 (HsRen H245), W267 (HsRen W288) and R280, which is apparently equivalent to HsRen R193, as both residues offer their guanidino group to a similar location in the active site. In both proteins, the active site cavity forms one end of an extended cleft to which β-NAD(P)-derived substrate(s) associate (Figure 1). Within this cleft are multiple hydrogen bonds and charge pairing interactions that in the *Pseudomonas* enzyme form a rather symmetrical set of interactions with respect to each nucleotide half of the substrate. However, the majority (8 of 11) form hydrogen bonding and/or charge pairing interactions with the pyrophosphate moiety of the substrate/product. Only one direct contact is observed for the nicotinamide amide and two for the 6 amino group of the adenine base with no hydrogen bonds from the protein engaging any of the hydroxyl groups of either ribose. This arrangement raises interesting questions about what part of the molecule contributes to the binding energy given that renalase must function in an environment in which non-substrate mono- and dinucleotides predominate. Using truncated forms of the substrate we offer evidence that, at least for human renalase, binding of the pyrophosphate moiety of the substrate has a primary contribution to stabilizing the pre-reduction E•S complex.

The substrate/product binding pose exposes one face of the ligand to direct interactions with solvent (Figure 1). Both the human (HsRen) and bacterial (PpRen) forms of renalase exhibit

a preference for substrates derived from β-NAD^+ over those derived from β-$NADP^+$ and this bias is notably more pronounced in the bacterial enzyme [14]. While this specificity bias is consistent with renalase serving to preferentially detoxify the inhibitory effect that 2DHNAD and 6DHNAD would exert on primary metabolism enzymes, the structural basis for this selectivity was hitherto unknown. In this study we present the structure of renalase from *Pseudomonas phaseolicola* in complex with β-NADPH and evaluate the influence of the ribose 2-phospho group in regard to the observed substrate specificity.

Materials and Methods

Materials

Dibasic potassium phosphate and sodium phosphate, monobasic potassium phosphate and sodium chloride were obtained from ACROS. β-NADH (disodium salt, trihydrate) was obtained from Amresco. β-NAD^+, β-$NADP^+$, nicotinamide mononucleotide (NMN), ADP-ribose, methyl nicotinamide and nicotinic acid were purchased from Sigma. Nicotinamide riboside (NR) was purchased from High Performance Nutrition. Renalases from *H. sapiens* (HsRen) and *P. phaseolicola* (PpRen) were expressed and purified according to previously published methods[14, 15]. Old yellow enzyme was prepared as previously described[2]. 6DHNAD and 6DHNADP were prepared and purified as described[2].

Preparation and analysis of reduced forms of NR and NMN

To establish whether nucleoside and nucleotide forms of 2-dihydro- and 6-dihydronicotinamides were substrates for renalase, 0.9 mL of a 300 μM solution of oxidized nicotinamide riboside (NR^+) or nicotinamide mononucleotide (NMN^+) was combined with 100 μL of a 3 mM solution of sodium borohydride in 100 mM potassium phosphate at pH 7.5. This resulted in instantaneous generation of the three reduced forms of each parent compound (2-, 4- and 6-dihydro). Each of these mixtures was divided in two and ~12.5 μM renalase (final) was added to one sample, while the other served both as unreacted and sample stability controls. All samples were incubated for 10 min prior to ultrafiltration using a 0.5 mL Amicon 10 kDa centrifugal filter to remove renalase. 50 μL of each filtrate was loaded onto an analytical Xbridge Peptide BEH C18 column (3.5 μM, 4.6 × 150 mm) run isocratically at 1.5 mL/min in 100 mM potassium phosphate at pH 7.5 with a Waters 600 pump coupled to a Waters 2487 dual wavelength detector, detecting simultaneously at 260 and 370 nm. The chromatographs obtained from samples to which renalase was added were corrected for the dilution.

For preparation of the 4DH forms of NR and NMN, sodium dithionite was used as a reductant in place of sodium borohydride [2]. 4DHNR and 4DHNMN were prepared by semi-preparative HPLC. The dithionite reduced mixtures were loaded onto a semi preparative Xbridge Prep C18 OBD column (5μM, 19 × 250 mm) run isocratically at 10 mL/min in 100 mM potassium phosphate buffer, pH 7.5 using a Waters 600 pump coupled to a Waters 2487 dual wavelength detector, detecting simultaneously at 260 and 340 nm. 4DHNR and 4DHNMN samples were frozen on dry ice during multiple collection cycles and then thawed and loaded onto a 35 cc Sep Pak (Waters) C18 cartridge equilibrated in 100 mM potassium phosphate pH 7.5. The bound sample and was eluted with water into 3 mL

fractions. The fractions that contained the desalted 4DHNR or 4DHNMN were pooled and immediately lyophylized. Once dry, the sample was dissolved in 6 mL of cold water and stored at −80 °C.

Spectrophotometric quantification of NAD analogs

Molar extinction coefficients for 2-, 4- and 6DHNMN and 2-, 4- and 6DHNR were determined by reducing a 4 mL solution containing ~20 mM NMN^+ or NR^+ in 100 mM potassium phosphate buffer, pH 7.5 with 1 mL of ~66 mM sodium borohydride solution prepared in 30 mM potassium phosphate buffer, pH 11. The resulting 5 mL solution containing all three reduced isomers was separated by semi-preparative HPLC as described above. Peaks corresponding to each of the reduced isomers were collected. Both 4- and 6-dihydro forms were frozen on dry ice while the less stable 2-dihydro isomers were used immediately. The concentration of each isomer was determined by the oxidase activities of renalase (2- and 6-dihydro forms) or old-yellow enzyme (4-dihydro form) using a Hansatech dioxygen electrode. Briefly, 1.6 mL of each sample collected was divided in two, where one half was used to obtain an absorption spectrum and the other was loaded into the oxygen electrode reaction vessel and allowed to react with either 10 μM renalase (2- and 6-dihydro NMN or NR) or 20 μM old yellow enzyme (4-dihydro NMN or NR). Based on each enzyme's reaction stoichiometry, the amount of oxygen consumed (μM) defined the concentration of the dihydronicotinamide substrate. This measurement was made three times for each isomer and the results were averaged after correction for the dilution that occurred with the addition of enzyme.

Reductive half-reactions with 2- and 6DHNMN and 2- and 6DHNR

Exclusion of dioxygen allows for observation of only the reductive half-reaction of renalase. Rate constants for reduction were determined using HsRen and PpRen as previously described [2, 14]. The post mixing concentration of HsRen was 6–11 μM and 2–5.5 μM for PpRen. Reduction of the renalase flavin cofactor was monitored at 458 nm for HsRen and 450 nm for PpRen. All half-reactions were carried out in 20 mM HEPES buffer, pH 7.5. Reactions with 2- and 6DHNR as substrates required the addition of the detergent octyl-beta-glucoside (2 mM final) in the tonometer to prevent excessive enzyme precipitation during the reaction. The reduction process was fit to equation 1 to obtain k_{obs} values. In this equation ΔA is the amplitude associated with the change in the enzyme's flavin absorption spectrum as it is reduced, k_{obs} is the observed rate constant for reduction of the flavin cofactor and C is the absorbance at infinite time. The k_{obs} values were then plotted against substrate concentration and fit to Equation 2 where the slope of the line gave k_{red}/K_d as a measure of the enzyme's substrate acquisition capacity, where k_{red} is the limit for the rate constant for reduction and K_d is the dissociation constant for the substrate, S.

$$A_{458}=\Delta A(e^{-k_{\mathrm{obs}}t})+C \quad \text{Equation 1}$$

$$k_{\mathrm{obs}}=(k_{\mathrm{red}}/K_d)[S] \quad \text{Equation 2}$$

The available concentration of 2DHNR and 2DHNMN was limited by instability. Samples could not be pooled and further purified, but were instead collected directly from the HPLC into a glass syringe containing D-glucose (1 mM final) and sparged with argon for 3 minutes. Glucose oxidase (10 μL, 1 U/μL) was added to the glass syringe immediately before mounting onto the stopped flow spectrophotometer to consume dissolved dioxygen.

Reductive half reactions were also undertaken in the presence of counterpart ligands. 2- and 6DHNMN and 2- and 6DHNR were used as substrates for renalase in the presence of AMP for NMN and ADP for NR. These experiments used double mixing stopped-flow spectrophotometry where renalase (HsRen, 10 μM and PpRen, 5 μM) was prepared anaerobically in 20 mM HEPES buffer, pH 7.5 and mixed with AMP or ADP and allowed to age for 100 ms before being mixed/reacted with 2- or 6DHNMN and 2- or 6DHNR respectively. Data were collected and analyzed as described above. Octyl-beta-glucoside (2 mM) was added to the enzyme solution for reactions containing 2- and 6DHNR.

Inhibition of human renalase by β-NAD(P), non-substrate analogs and fragments

The 50% inhibitory concentration (IC_{50}) of NAD fragments: ADP, ADP-ribose, AMP, nicotinamide, methyl nicotinamide, NR^+, NMN^+, 4DHNR, and 4DHNMN, were estimated by observing the renalase reductive half reaction in the absence of dioxygen and in the presence of a 6DHNAD concentration that was equal to the measured dissociation constant for that substrate (173 μM)[2]. Renalase (~4–6 μM) in 2X PBS buffer containing 1 mM D-glucose was added to the main chamber of a tonometer and glucose oxidase (25 μL, 1 U/μL) was added to the side arm prior to assembly and was kept at 4 °C. The tonometer was assembled and made anaerobic by exchanging argon for dissolved oxygen using partial vacuum followed by equilibration with high purity argon gas (5 psi) that was passed through an Alltech oxygen-reactive cartridge and sparged through anaerobic water. This process was repeated for 45 cycles where after every 3 cycles the sample was agitated during the introduction of argon gas to enhance the exchange of dissolved gases. The glucose oxidase and D-glucose/renalase solutions were combined and the tonometer was mounted on a Hitech Scientific (now TgK) DX2 stopped-flow spectrophotometer that had been scrubbed of dioxygen for >12 hrs using an anaerobic solution of 50 mM D-glucose and 15 U/mL glucose oxidase in 20 mM HEPES buffer, pH 7.0. Concentrated 6DHNAD was aliquoted to yield 173 μM after the second mixing step (four-fold dilution) and stored at −80 °C to prevent decomposition. Each aliquot was thawed and diluted to 3 mL in water containing 1 mM D-glucose. The solution containing 6DHNAD was transferred to a glass syringe and made anaerobic by sparging with high purity argon gas for 4 minutes. Glucose oxidase (10 μL, 1 U/μL) was added to the syringe immediately prior to capture and mounting onto the stopped-flow spectrophotometer. Potential inhibitory ligands were prepared in 2X PBS with 1 mM D-glucose, transferred into a glass syringe and made anaerobic as described above for 6DHNAD. The renalase solution was mixed first with the NAD analog (or fragment) solution and allowed to age for 100 ms before being mixed with the substrate (6DHNAD) solution. Reduction of the renalase flavin cofactor was observed at 458 nm. The data were fit to a single exponential decay according to equation 1 using Kinetic Studio software (TgK Ltd). The dependence of the observed rate constant on the concentration of the analog was fit to Equation 3 to determine the IC_{50} value for each. In this equation k_{max} is the rate

constant for reduction in the absence of inhibitory ligand and k_{min} is the observed rate constant with saturating inhibitory ligand (this value was manually set to zero for cases in which the inhibitory ligand had a solubility limit lower than the concentration required to saturate the enzyme).

$$\nu = k_{min} + \frac{k_{max} - k_{min}}{(1 + (\frac{[6DHNAD]}{K_i})} \quad \text{Equation 3}$$

Crystallization, structure determination, and model refinement of the PpRen•β-NADPH complex

Crystallization conditions for PpRen were those identified initially by the North East Structural Genomics Consortium that yielded the unliganded enzyme structure, PDB ID 3KKJ: 2 M sodium formate, 100 mM sodium acetate pH 4.6 at 20 °C. Diffraction-quality crystals were obtained by the hanging drop vapor diffusion method. The droplet was formed from 1 μL of the well solution and 1 μL of PpRen (104 μM). Crystals grew within 1–2 days to dimensions of ~200 μm × 50 μm × 10 μm. Individual crystals were lifted from the drops using nylon cryo-loops, and soaked for 1–3 minutes in 2.5 M sodium formate, 125 mM sodium acetate pH 4.7 with 10% glycerol and 40 mM β-NADPH. The loop-mounted, cryo-solution and crystal were cooled to form a glass by immersion in liquid nitrogen. X-ray diffraction data to 2.1 Å for the PpRen•β-NADPH complex were collected at beamline 21-ID-F of the Life Science Collaborative Access Team (LS-CAT) at the Advanced Photon Source (APS) at a wavelength of 0.97872 Å at 100 K. The crystal was rotated through 190°, with an oscillation angle of 0.4°. The exposure time per frame was 0.75 s with 0% attenuation. The crystal to detector distance was 220.2 mm. Data were indexed and scaled with HKL2000 [16] in space group $P2_1$ with unit cell dimensions a=63.4 Å, b=71.0 Å, c=74.8 Å, and β=107.8 °.

The structure of PpRen•β-NADPH was determined by molecular replacement in PHASER[17] with a search model derived from chain A of the *P. phaseolicola* renalase•β-NADH structure (PDB ID 4ZCC)[14] with all non-protein atoms removed and all B-factors set to 20.0 $Å^2$. After iterative cycles of manual model building in COOT[18] and maximum likelihood based refinement using the PHENIX package (phenix.refine)[19], ordered solvent molecules were added automatically in phenix.refine and culled manually in COOT. After adding solvent atoms, the FAD cofactor and β-NADPH were added to the model. During the last rounds of refinement, hydrogen atoms were added to the model using phenix.reduce[20] to improve the stereochemistry of the model. Positions of H atoms were refined using the riding model with a global B-factor. Regions of each model to be used in translation-libration-screw (TLS) refinement were identified using phenix.find_tls_groups and the TLS parameters were refined in phenix.refine. Once the refinement converged, the model was validated using the tools implemented in COOT and PHENIX[21],[22]. Side chains with poor or missing electron density were modeled in favored rotameric conformations. The B-factors were allowed to refine without additional restraints, and the occupancies were held to 1.0. Data collection and model refinement statistics are listed in Table 1.

Structure determination, and model refinement of the MDH•6DHNAD and LDH•6DHNAD complexes

E. coli malate dehydrogenase (MDH) was prepared as previously described[2]. MDH crystal growth was carried out by the hanging drop method at 18 °C. Drops containing 1.5 μl of purified MDH protein at 80 μM containing 0.4 mM 6DHNAD were mixed with equal volumes of a reservoir solution containing 0.1 M MES, pH 6.5, 21% PEG 8,000. Large crystals (400 × 200 × 50 μm) formed in 1–2 weeks[23]. For data collection, crystals were retreived with a nylon cryo-loop and washed with 0.1 M MES, pH 6.5, 21% PEG 8,000, 0.5 mg/ml MDH supplemented with 20% (v/v) glycerol as a cryoprotectant. The cryo-solution and crystal were cooled to form a glass by immersion in liquid nitrogen.

L-lactate dehydrogenase (LDH) from rabbit muscle was purchased from Sigma-Aldrich as an ammonium sulfate suspension. The suspension was diluted five-fold with 50 mM HEPES, pH 7.5, 50 mM NaCl, 1 mM DTT, desalted using a PD-10 column (GE Healthcare) into the same buffer, and concentrated to 410 μM. LDH crystal growth was carried out by the hanging drop method at 18 °C. A volume of 1.5 μL of LDH protein containing 1.2 mM 6DHNAD was mixed with an equal volume of a reservoir solution containing 0.1 M Tris buffer, pH 7.5, 0.1 M sodium acetate, 15% PEG 8,000. Large crystals (400 × 300 × 100 μm) formed in 3–4 days. For data collection, crystals were soaked with 0.3 μL of 9.3 mM 6DHNAD for 40 minutes and washed with 0.1 M Tris buffer, pH 7.5, 0.05 M sodium acetate, 14% PEG 8,000 supplemented with 25% (v/v) PEG 400 as a cryoprotectant and flash cooled in liquid nitrogen. Data collection and model refinement statistics are listed in Table 1.

All MDH and LDH diffraction data were collected at the Stanford Synchrotron Radiation Laboratory (SSRL; Stanford, CA), beamline 9-2. MDH•6DHNAD diffraction data were collected (0.2° oscillation images for a total of 131°) at a wavelength of 0.9795 Å at 100 K. The exposure time per frame was 2.83 s with 0 % attenuation and a crystal to detector distance of 280.2 mm. The data were indexed and scaled with XDS to 1.75 Å. The crystals were assigned to the space group $P2_12_12_1$ with unit cell dimensions a = 77.5 Å, b = 83.8 Å, c = 89.3 Å. Molecular replacement calculations for MDH were performed using PHASER in the PHENIX program suite[24, 25], using molecule A of 3HHP[26] as the search model with waters removed, yielding a clear solution with a log-likelihood gain of 9,078 and a TFZ score of 89.0. Model building and refinement were performed in iterative cycles using COOT[27] and phenix.refine. The MDH structure model includes residues 1–78, 90–311 in molecule A and 1–79, 90–311 in molecule B of 312 total residues. The model includes two 6DHNAD molecules, one in each NADH binding site, and 473 water molecules.

LDH•6DHNAD diffraction data (0.2° oscillation images for a total of 180°) were collected with a wavelength of 0.9795 Å at 100 K. The exposure time per frame was 0.860 s with 0% attenuation and a crystal to detector distance of 285.3 mm. The data were indexed and scaled with XDS to 1.86 Å. The crystals were assigned to the space group $P2_1$ with unit cell dimensions a = 63.6 Å, b = 126.1 Å, c = 84.2 Å, and β = 99.9°. Data collection and model refinement statistics are listed in Table 1. Molecular replacement calculations for LDH were performed using PHASER in the PHENIX program suite, using molecule A from 4I9H[28] as the search model with ligand and waters removed yielding a clear solution with a log-

likelihood gain of 15,192 with a TFZ score of 86.9. Model building and refinement were performed using COOT and phenix.refine. The LDH structure model includes residues 1–13, 17–331 in molecule A; 2–98, 109–331 in molecule B; 2–13, 17–329 in molecule C; and 1–329 in molecule D of 331 total residues. The model also includes 4 6DHNAD molecules, one in each β-NADH-binding site. The 6DHNAD in molecule D was best modeled with two orientations of the adenine ring. There are 506 water molecules and 5 sulfates modelled. The sulfate ions were derived from the ammonium sulfate suspension in which the protein was purchased.

Structural analysis

Protein structure figures were generated using PyMOL [29]. The atomic coordinates and structure factors have been deposited in the Protein Data Bank (Research Collaboratory for Structural Bioinformatics, Rutgers University, New Brunswick, NJ) as entries 5KKA for the MDH•6DHNAD structure, 5KKC for the MDH•6DHNAD structure and 5KRQ for the PpRen•β-NADPH structure.

Single crystal spectrophotometry

In order to verify that the MDH•6DHNAD and LDH•6DHNAD structures contained 6DHNAD and not a decomposition product of this relatively unstable molecule, absorption spectra where recorded from the same crystals of these complexes that were used for structural elucidation. Absorbance spectra (220–500 nm) were recorded on SSRL beamline 9-2 by measuring counts for dark (D) and reference (R) scans adjacent to the crystal and then focusing the beam on the crystal or sample (S) to measure transmittance. Absorption spectra were then obtained according to equation 4.

$$A=\log_{10}[(R-D)/(S-D)] \quad \text{Equation 4}$$

A five-axis pico-motor stage was used to align the microspec objective lenses with each other and three larger stages were used to align the pair of objectives to the sample position. An approximately 50 μm diameter circular beam was used. The system used a Hamamatsu light source with both deuterium and halogen lamps, UV solarization-resistant optical fibers, reflective Newport Schwardchild objectives, and an Ocean Optics QE65000 Spectrum Analyzer.

Results

HPLC substrate analysis of 2-, 4- and 6DHNMN and 2-, 4- and 6DHNR

All three reduced isomers of NR and NMN were reacted with renalase to determine which were substrates. Control reactions were run in the absence of enzyme to define initial reference concentrations and account for losses due to decomposition. Analysis of the chromatographs obtained indicated that, much like the β-NAD(P)-derived substrates, only 2- and 6DHNR and 2- and 6DHNMN are consumed by renalase (Figure 2 A and C). The extinction coefficient spectrum for the dihydronicotinamide chromophore was determined for each reduced form using spectrophotometry in conjunction with a dioxygen electrode.

This procedure yielded extinction coefficients of ε_{338nm} = 7100 ± 300 M^{-1} cm^{-1} for 4DHNMN, ε_{338nm} = 7300 ± 200 $M^{-1}cm^{-1}$ for 6DHNMN, ε_{391nm} = 7000 ± 100 $M^{-1}cm^{-1}$ for 2DHNMN, ε_{340nm} = 7200 ± 100 $M^{-1}cm^{-1}$ for 4DHNR, ε_{345nm} = 10400 ± 600 $M^{-1}cm^{-1}$ for 6DHNR and ε_{389nm} = 8700 ± 500 $M^{-1}cm^{-1}$ for 2DHNR (Figure 2 B and D).

Reductive half-reactions and the effect of complimentary ligands with 2- and 6DHNR and 2- and 6DHNMN

We have previously reported that 2- and 6DHNAD(P) molecules are substrates for renalase. Here we report data for reductive half reactions of renalase from both *H. sapiens* and *P. phaseolicola* with 2- and 6DHNR and 2- and 6DHNMN as substrates (Figure 2) with and without the complimentary co-ligand of each: ADP or AMP, respectively (Figure 3). Similar to the β-NAD- and β-NADP-derived substrates, the 6DH isomers of NR and NMN proved sufficiently stable to be purified, desalted and stored as described above and the 2DH isomers were considerably less stable, dictating that they be used immediately after elution from preparative HPLC. As such the concentration of the 2DH substrates was limited by the ability of the semi preparative C18 column to resolve the 2DH isomer from other species present (~100 μM for 2DHNR and 2DHNMN). Observation of the reduction of the flavin cofactor (458 nm for HsRen and 450 nm for PpRen) by 2- and 6DHNR and 2 and 6NMN in the presence or absence of the respective compliment ligand (ADP for nicotinamide riboside species or AMP for nicotinamide mononucleotide) was carried out under anaerobic conditions at 25 °C. The complimentary ligand at high concentration (generally limited by solubility) was mixed with renalase in the first mixing step and allowed to age for 100 ms. Reduction experiments used largely pseudo-first order concentration ranges: 6DHNR (57 to 949 μM), 6DHNMN (78 to 675 μM), 2DHNR (32 μM to 105 μM) and 2DHNMN (47 μM to 83 μM). These data were fit to a single exponential decay to obtain a measure of observed rate constant values (Equation 1).

Plotting k_{obs} data versus the concentration of substrate (2- and 6DHNR +/− ADP, 2- and 6DHNMN +/− AMP) gave a linear dependence for all data sets, where the slope is k_{red}/K_d. A linear dependence suggests that the reduction reaction is reliant on relatively weak binding interactions for these substrates, and the concentrations attained were insufficient to show curvature in the dependence plot that would be indicative of pre-equilibrium binding. For PpRen the addition of complementary or counterpart ligands (AMP for NMN, ADP for NR) had no significant effect. For HsRen, addition of ADP (4–5 mM) in together with 6DHNR resulted in a 7-fold increase in k_{red}/K_d (Figure 3), but the equivalent analysis for 2- and 6DHNMN with HsRen with the AMP counterpart ligand showed no measurable difference for k_{red}/K_d. These data suggest that the β−phosphate of bound ADP induces a conformation change that aids in hydride transfer from 6DHNMN to the Flavin. More generally, however, the data show that untethered occupancy of the distal portions of the dinucleotide binding site do not dramatically enhance the rate of hydride transfer. For all substrates, maximal rates for hydride transfer are observed with intact dinucleotides.

Inhibition of renalase by β-NAD(P) analogs

Dissociation constants for non-substrate fragments and isomers were measured by determination of the 50% suppression (IC_{50}) of the observed rate constant for reduction in

the presence of a substrate (6DHNAD) concentration equal to the K_d for that substrate (a concentration that was also pseudo-first order with respect to the enzyme concentration). For those molecules that were inhibitory, IC_{50} values were calculated by fitting a plot of k_{obs} for reduction versus the concentration of the substrate fragments, AMP, ADP, ADP-ribose, nicotinamide, methyl nicotinamide, NR or NMN to equation 3 (Figure 4). This analysis was hampered to some extent by apparent IC_{50} values greater than or similar to the solubility limit for these molecules. However, the data show that it is generally the case that the phospho-group proximal to the nicotinamide has a greater contribution to ligand binding than does the distal. With the exception of 4DHNR, molecules that did not contain this proximal phospho group, such as AMP, nicotinamide and methyl nicotinamide, did not show measureable inhibition of 6DHNAD oxidation. However, derivatives that did contain the proximal phosphate, ADP, ADP-ribose and 4DHNMN, displayed observable inhibition yielding estimated K_d values of 15, 12.4 and 1 mM, respectively. Titration of oxidized forms of NR and NMN did not yield any substrate inhibition even though the 4-dihydro form of both molecules was observed to be inhibitory. Moreover, the products (β-NAD^+ and β-$NADP^+$) have been shown to bind with low millimolar binding constants. This likely reflects competing cumulative interactions at the active site and along the ligand binding cleft. The positive charge of the oxidized nicotinamide is likely repelled from the active site by the local positive electrostatic environment adjacent to the nicotinamide binding site resulting from conserved histidine and arginines (Figure 1), and we have proposed in prior work that this potential aids product dissociation[14]. Truncated and reduced non-substrate isomers (4DHNR, 4DHNMN) avoid this repulsive influence but cannot form other interactions with the AMP/ADP moiety that would aid binding. We therefore conclude that, in the oxidized state (NR^+ and NMN^+), the active site charge-repulsion is dominant over other binding interactions.

The PpRen•NADPH complex

Our prior investigation of renalase from *P. phaseolicola* indicated that this form of renalase exhibited a pronounced substrate preference profile. The bacterial enzyme reacted with 2DH-substrates 160 to 350-fold more rapidly than 6DH-substrates. This bias seemed to be accounted for by a hydrogen bond from the nicotinamide amide to threonine 185 that stabilized a substrate binding pose in which the 2-dihydro hydride was proximal (3.6 Å) and the nicotinamide ring parallel to the flavin N-5 (Figure 1)[14]. As mentioned above, this form of renalase also bound β-NAD-derived substrates (6DH and 2DH) and non-substrates (4DH) 15 to 50-fold more tightly than those derived from β-NADP, indicating that the added 2'-phosphoryl group impedes binding by 6–10 kJ/mole. Such a substrate binding preference would be expected if the function of renalase is to ameliorate the inhibitory threat to primary metabolism where β-NAD is the predominant nicotinamide dinucleotide co-substrate. The structural basis for this substrate preference is described here with the structure of the PpRen•β-NADPH complex, which was solved to 2.1 Å-resolution (Figure 5). This structure is very similar to the PpRen•β-NADH structure (4ZCC) we previously published, however, the nicotinamide nucleoside moiety is disordered and not visible in the electron density maps. The most striking aspect of this structure is that the NADPH 2'-phosphoryl group does not appear to interact favorably or unfavorably, with regard to binding, with any residue from the protein. While it is near the terminal amide of glutamine 206 (3.4 Å), the β-carbon

of phenylalanine 204 (3.9 Å) and aspartate 211(~6.0 Å), none of these residues are oriented to form energetically significant binding interactions. It therefore seems likely that for the bacterial enzyme β-NADP-derived ligands are to a greater extent partitioned into the aqueous medium than those derived from β-NAD and that this is the basis for the NAD vs NADP ligand selectivity.

The MDH•6DHNAD and LDH•6DHNAD complexes

The final composite omit maps for the MDH•6DHNAD or LDH•6DHNAD structures showed that two 6DHNAD inhibitor complex structures were obtained. The MDH•6DHNAD structure was refined to 1.75 Å-resolution and the LDH•6DHNAD structure was refined to 1.86 Å-resolution (Figure 6). These structures indicate, as might be predicted, that 6DHNAD occupies the NAD(H)-binding site of both enzymes and does not appear to promote the binding of the respective co-substrate. As a consequence of the high affinity of 6DHNAD for MDH and LDH, these structures serve as two examples of the inhibitory threat posed by non-specific reduction of NAD^+ molecules.

There are four structures of MDH available on the PDB database; MDH•NAD^+ (1IB6), MDH•NAD^+•pyruvate (1IE3), MDH•NAD^+•citrate (1EMD), and a high resolution structure of the unliganded enzyme (3HHP)[23, 30, 31]. The binding of the 6DHNAD to MDH is positionally identical to the other published MDH•NAD structures with the exception of MDH•NAD^+•citrate (1EMD) where the nicotinamide ring is pivoted to accommodate the citrate. While the omit map suggests a small pucker of the nicotinamide ring at position 6, cyclohexadiene or piperidine-diene rings do not normally have appreciable out of plane distortions. The overall structure of the MDH molecules from all of the structures (those published and those presented here) are very similar, with the only difference being in the loop (residues 81 – 90) that closes over the active site when citrate (or sulfate) is present (1EMD, 1IB6). This loop is open in the MDH•6DHNAD structure presented here (5KKA), in the prior unliganded structure (3HHP), and in the structure with pyruvate (1IE3). This loop is disordered in several of the MDH molecules in the asymmetric units of these structures, whether there is substrate bound or not.

There are also several structures of LDH in the PDB. There is a prior structure of the rabbit muscle LDH•NAD•oxamate ternary complex (3H3F) and 4 other structures with a variety of inhibitors bound[32]. There is also a structure of the human muscle LDH•NAD•oxalate complex (4OKN)[33]. The structure of rabbit muscle LDH•6DHNAD presented here aligns well with both the rabbit and human structures and the NAD aligns well in all of the structures. The 6DHNAD in the LDH structure presented here (5KKC) also appears to have a small pucker in the nicotinamide ring. Similar to the MDH structures, there is a loop that closes over the active site (residues 97–107) that is disordered in all of the molecules of our structure's asymmetric unit, but is seen in the open and closed positions in the other two structures, irrespective of whether there is a substrate analog or inhibitor bound.

6DHNAD Crystal Occupancy from Single Crystal Spectrophotometry

6DHNAD is a relatively unstable molecule that degrades with a half-life of around 24 hours under the conditions used for crystallization (data not shown). For both the MDH•6DHNAD

and LDH•6DHNAD structures, the crystals were formed by co-crystallization with the inhibitory ligand. LDH was exposed to the ligand again prior to mounting in the loop during cryo-protection. To verify occupancy of 6DHNAD in both the MDH and LDH structures, single crystal spectrophotometry was performed on both complexes (Figure 6). For both MDH and LDH, the the extinction coefficient of the 6DHNAD nicotinamide increases when bound. For the MDH•6DHNAD complex the 6DHNAD λmax shifts from 345 nm to ~360 nm, while for the LDH•6DHNAD complex the 6DHNAD dihydronicotinamide λmax wavelength is largely unaltered when bound to the enzyme. For the MDH•6DHNAD complex the extinction coefficient of the dihydronicotinamide absorption transition increases by a factor of 1.14, while for the LDH•6DHNAD complex it increases by a factor of 1.23. Both crystals exhibited far UV absorption features indicative of a bound dihydronicotinamide establishing that 6DHNAD occupies the active site of the crystals used to solve the MDH and LDH structures presented.

Discussion

The data presented here and in prior work are consistent with an intracellular housekeeping function for renalase. Non-specific reduction of N-substituted nicotinamides (chiefly $NAD(P)^+$) yields three forms of the dihydronicotinamide base. We have shown that two such isomers derived from reduction of NAD^+ are inhibitors of enzymes that require NADH molecules as substrates. Renalase serves to oxidize these inhibitory isomers and recycle them by forming $NAD(P)^+$ (Scheme 1). Prior work has shown that renalases isolated from different kingdoms have the same activity but unique structural features and substrate specificity profiles [13, 14]. In this study we present data that accounts for some aspects of the specificity profile of human and bacterial renalase, explore binding to the active site using analog and truncated substrate and non-substrate molecules, and also offer structures of one inhibitory NADH isomer (6DHNAD) bound to two primary metabolism dehydrogenases.

To date, only Human (HsRen) and *Pseudomonas* (PpRen) forms of renalase have been identified. The structures of these enzymes indicate that the portion of the active site of renalase that interacts with the FAD isoalloxazine and substrate/product nicotinamide has few conserved residues. For both forms of the enzyme, the remainder of the active site is an extended cleft on the surface of the protein. Ligand-bound structures of PpRen indicate that this cleft accommodates the remainder of the substrate and forms apparent hydrogen bonds and charge pairing interactions with the phospho groups and the adenine base; moieties that are common to all mono- and dinucleotide substrates and/or cofactors (Figure 1). Renalase functions in an intracellular environment in which potentially competing inhibitory ligands predominate (AMP, ADP, ATP, NADH, NADPH, 4DHNR & 4DHNMN) relative to the concentration of available substrates (6DHNAD, 2DHNAD, 6DHNAP, 2DHNADP, 6DHNR, 2DHNR, 6DHNMN and 2DHNMN), that are assumed to be maintained at low concentration by the irreversible oxidase activity of renalase. Our data indicate that non-substrate ligands tend to either bind weakly (or possibly do not bind) to renalase (Figure 4). Nicotinamide ribosides and nucleotides are predominantly found in four forms in the cell: NAD, NADP, NR and NMN. We have shown that the 2- and 6-dihydronicotinamides of each of these molecules are substrates for renalase [2] (Figure 2) and that renalase has the capacity to

kinetically select against oxidizing 4-dihydronicotinamide substrates by positioning the nicotinamide such that the FAD N5, the presumed site for hydride transfer [34], is distant from the 4-position of the nicotinamide [14]. The NR and NMN substrates bind to renalase weakly (Figure 3), to the extent that no curvature was observed in the plot of the observed rate constant for reduction versus substrate concentration, suggesting quasi-collision based chemistry within the limited range of substrate concentration available to assess these dependencies (Figure 3). However, these molecules behave as substrates as they reduce the renalase cofactor approximately 5-orders of magnitude more rapidly than does β-NADH (4DHNAD). If the substrate forms of NR and NMN bound in the same conformation as that portion of β-NAD(P)(H) observed in the PpRen•β-NADH and PpRen•β-NAD^+ structures[14], NR could make only one hydrogen bond and NMN would form a maximum of two hydrogen bonds and two complementary charge-pair interactions accounting for the six-fold difference in the K_d for 4DHNMN compared to 4DHNR (Figure 1). One curiosity that was observed for HsRen is that the simultaneous addition of a high concentration of the complement co-ligand (ADP for NR) stimulated the rate of reduction by a factor of seven for 6DHNR. This emphasizes that the substrate-binding sites in HsRen and PpRen are fundamentally different and suggests that, for HsRen, catalysis can be enhanced by occupancy of the distant portions of the substrate binding cleft relative to the site of hydride transfer. Moreover, it suggests that for HsRen an intact pyrophosphate moiety increases the rate of reduction.

The structure of the PpRen•β-NADPH complex was solved to account for the unique specificity profile of the bacterial enzyme. PpRen exhibits a 6–10 kJ/mol preference to bind NAD-derived molecules compared to NADP-derived ligands [14]. The structure of the PpRen•β-NADPH complex indicates that the 2'-phospho-group of β-NADPH does not interact in a manner conducive to binding with any residue on the surface of the enzyme. As such, there is no partner residue to satisfy the negative charge of the phospho group, dictating that this charged moiety would retain its hydration shell when bound to PpRen. Such a binding pose would mean that β-NADPH would be fractionally more partitioned into bulk solvent when bound, undermining its capacity to remain associated. Comparing HsRen and PpRen, β-NAD and NADP-derived ligands bind with similar affinity to HsRen [2], whereas PpRen binds NAD-derived ligands with dissociation constants that indicate 13 to 50-fold higher affinity than for ligands derived from NADP [14]. This difference in dinucleotide specificity is potentially accounted for by the presence of an arginine (Arg222) in HsRen whose guanidino group is adjacent the position occupied by the 2'-phospho group (as observed in the PpRen•β-NADPH structure; Figure 1). In the equivalent position of the PpRen•β-NADPH structure is an aspartate residue (Asp211) whose carboxylate resides 6.0 Å from the β-NADPH 2'-phospho group.

In prior studies, we demonstrated that 2- and 6DHNAD molecules were competitively inhibitory to specific enzymes that have β-NADH as substrate [2]. The assumption was that the isomeric forms are sufficiently similar in shape and charge distribution to mimic β-NADH molecules. These isomers bound with K_i values in the sub-micromolar range with *E.coli* malate dehydrogenase exhibiting a K_i of 34 nM for 6DHNAD. Here we present the structures of *E.coli* malate dehydrogenase and rabbit muscle lactate dehydrogenase bound to 6DHNAD. Instability of the 2- and 6DHNAD molecules dictates that we verify that these

molecules are present in the structures as solved. To do this we used the dihydro-nicotinamide chromophore to observe the absorption of the ligand by single crystal spectrophotomtery (Figure 6). The spectra obtained indicate that both the MDH and LDH structures were solved with 6DHNAD bound (given that this was the only reduced form of NAD added). As may be readily predicted, 6DHNAD occupies the binding site for β-NADH/β-NAD^+ in these enzymes [31, 32], convincingly demonstrating two examples of the mode of competitive inhibition of primary metabolism enzymes by 6DHNAD and by extension 2DHNAD molecules.

Acknowledgments

This publication was made possible by funds from National Science Foundation grants numbered CHE-1402475 (G.R.M.), CHE-1403293 (A.L.L.) and MCB-1157392 (N.R.S), National Institutes of Health grant numbered K02 AI093675 from the National Institute for Allergy and Infectious Disease (A.L.L.) and by a UWM Research Growth Initiative Grant (G.R.M.).

Abbreviations

ADP	adenosine diphosphate
ADP-ribose	adenosine diphosphate ribose
AMP	adenosine monophosphate
β-NAD^+	oxidized nicotinamide adenine dinucleotide
β-$NADP^+$	oxidized nicotinamide adenine dinucleotide phosphate
β-NADPH	reduced nicotinamide adenine dinucleotide phosphate
FAD	flavin adenine dinucleotide
HPLC	high performance liquid chromatography
HsRen	renalase from *H. sapiens*
NMN	nicotinamide mononucleotide
NR	nicotinamide riboside
PpRen	renalase from *P. phaseolicola*
6DHNAD	6-dihydronicotinamide adenine dinucleotide
2DHNAD	2-dihydronicotinamide adenine dinucleotide
6DHNADP	6-dihydronicotinamide adenine dinucleotide phosphate
2DHNADP	2-dihydronicotinamide adenine dinucleotide phosphate
4DHNMN	4-dihydronicotinamide mononucleotide
6DHNMN	6-dihyronicotinamide mononucleotide
2DHNMN	2-dihydronicotinamide mononucleotide

4DHNR	4-dihydronicotinamide riboside
6DHNR	6-dihydornicotinamide riboside

References

1. Godtfredsen SE, Ottesen M. 1,6-Dihydro-NAD as an Humidity-Induced Lactate Dehydrogenase Inhibitor in NADH Preparations. Carlesberg Research Communications. 1978; 43:171–175.
2. Beaupre BA, Hoag MR, Roman J, Forsterling FH, Moran GR. Metabolic Function for Human Renalase: Oxidation of Isomeric Forms of beta-NAD(P)H that Are Inhibitory to Primary Metabolism. Biochemistry. 2015; 54(3):795–806. [PubMed: 25531177]
3. Luft FC. Renalase, a catecholamine-metabolizing hormone from the kidney. Cell Metab. 2005; 1(6): 358–60. [PubMed: 16054084]
4. Xu J, Li G, Wang P, Velazquez H, Yao X, Li Y, Wu Y, Peixoto A, Crowley S, Desir GV. Renalase is a novel, soluble monoamine oxidase that regulates cardiac function and blood pressure. The Journal of clinical investigation. 2005; 115(5):1275–80. [PubMed: 15841207]
5. Gosh RR, Gehr TWB, Sica DA, Masilamani S, Fakhry I, Wang R, Mcquire E, Gosh S. Effect of renalase inhibition on blood pressure. J Am Soc Nephrol. 2006; 17:208A. (abstract). [PubMed: 16221868]
6. Desir GV. Renalase deficiency in chronic kidney disease, and its contribution to hypertension and cardiovascular disease. Curr Opin Nephrol Hypertens. 2008; 17(2):181–5. [PubMed: 18277152]
7. Li G, Xu J, Wang P, Velazquez H, Li Y, Wu Y, Desir GV. Catecholamines regulate the activity, secretion, and synthesis of renalase. Circulation. 2008; 117(10):1277–82. [PubMed: 18299506]
8. Guo X, Wang L, Velazquez H, Safirstein R, Desir GV. Renalase: its role as a cytokine, and an update on its association with type 1 diabetes and ischemic stroke. Curr Opin Nephrol Hypertens. 2014; 23(5):513–8. [PubMed: 24992568]
9. Wang L, Velazquez H, Chang J, Safirstein R, Desir GV. Identification of a receptor for extracellular renalase. PLoS One. 2015; 10(4):e0122932. [PubMed: 25906147]
10. Guo X, Hollander L, MacPherson D, Wang L, Velazquez H, Chang J, Safirstein R, Cha C, Gorelick F, Desir GV. Inhibition of renalase expression and signaling has antitumor activity in pancreatic cancer. Sci Rep. 2016; 6:22996. [PubMed: 26972355]
11. Hollander L, Guo X, Velazquez H, Chang J, Safirstein R, Kluger HM, Cha C, Desir G. Renalase expression by melanoma and tumor associated-macrophages promotes tumor growth through a STAT3-mediated mechanism. Cancer Res. 2016
12. Desir GV. Renalase is a novel renal hormone that regulates cardiovascular function. J Am Soc Hypertens. 2007; 1(2):99–103. [PubMed: 20409839]
13. Milani M, Ciriello F, Baroni S, Pandini V, Canevari G, Bolognesi M, Aliverti A. FAD-binding site and NADP reactivity in human renalase: a new enzyme involved in blood pressure regulation. Journal of molecular biology. 2011; 411(2):463–73. [PubMed: 21699903]
14. Hoag MR, Roman J, Beaupre BA, Silvaggi NR, Moran GR. Bacterial Renalase: Structure and Kinetics of an Enzyme with 2- and 6-Dihydro-beta-NAD(P) Oxidase Activity from Pseudomonas phaseolicola. Biochemistry. 2015; 54(24):3791–802. [PubMed: 26016690]
15. Beaupre BA, Carmichael BR, Hoag MR, Shah DD, Moran GR. Renalase Is an alpha-NAD(P)H Oxidase/Anomerase (JACS Spotlight Article). Journal of the American Chemical Society. 2013; 135(37):13980–7. [PubMed: 23964689]
16. Otwinowski Z, Minor W. Processing of X-ray diffraction data collection in oscillation mode. Methods Enzymol. 1997; 276:307–325.
17. McCoy AJ, Grosse-Kunstleve RW, Adams PD, Winn MD, Storoni LC, Read RJ. Phaser crystallographic software. J Appl Crystallogr. 2007; 40(Pt 4):658–674. [PubMed: 19461840]
18. Emsley P, Lohkamp B, Scott WG, Cowtan K. Features and development of Coot. Acta Crystallogr D Biol Crystallogr. 2010; 66(Pt 4):486–501. [PubMed: 20383002]

19. Afonine PV, Mustyakimov M, Grosse-Kunstleve RW, Moriarty NW, Langan P, Adams PD. Joint X-ray and neutron refinement with phenix.refine. Acta Crystallogr D Biol Crystallogr. 2010; 66(Pt 11):1153–63. [PubMed: 21041930]
20. Word JM, Lovell SC, Richardson JS, Richardson DC. Asparagine and glutamine: using hydrogen atom contacts in the choice of side-chain amide orientation. J Mol Biol. 1999; 285(4):1735–47. [PubMed: 9917408]
21. Urzhumtseva L, Afonine PV, Adams PD, Urzhumtsev A. Crystallographic model quality at a glance. Acta Crystallogr D. 2009; 65:297–300. [PubMed: 19237753]
22. Chen VB, Arendall WB 3rd, Headd JJ, Keedy DA, Immormino RM, Kapral GJ, Murray LW, Richardson JS, Richardson DC. MolProbity: all-atom structure validation for macromolecular crystallography. Acta Crystallogr D Biol Crystallogr. 2010; 66(Pt 1):12–21. [PubMed: 20057044]
23. Zaitseva J, Meneely KM, Lamb AL. Structure of Escherichia coli malate dehydrogenase at 1.45 A resolution. Acta crystallographica. 2009; 65(Pt 9):866–9. [PubMed: 19724119]
24. Adams PD, Afonine PV, Bunkoczi G, Chen VB, Davis IW, Echols N, Headd JJ, Hung LW, Kapral GJ, Grosse-Kunstleve RW, McCoy AJ, Moriarty NW, Oeffner R, Read RJ, Richardson DC, Richardson JS, Terwilliger TC, Zwart PH. PHENIX: a comprehensive Python-based system for macromolecular structure solution. Acta crystallographica. Section D, Biological crystallography. 2010; D66(Pt 2):213–21.
25. Afonine PV, Grosse-Kunstleve RW, Echols N, Headd JJ, Moriarty NW, Mustyakimov M, Terwilliger TC, Urzhumtsev A, Zwart PH, Adams PD. Towards automated crystallographic structure refinement with phenix.refine. Acta crystallographica. 2012; 68(Pt 4):352–67.
26. Zaitseva J, Meneely KM, Lamb AL. Structure of Escherichia coli malate dehydrogenase at 1.45 A resolution. Acta Crystallogr Sect F. 2009; 65(Pt 9):866–9.
27. Emsley P, Cowtan K. Coot: model-building tools for molecular graphics. Acta Cryst. 2004; D60(Pt 12 Pt 1):2126–32.
28. Kohlmann A, Zech SG, Li F, Zhou T, Squillace RM, Commodore L, Greenfield MT, Lu X, Miller DP, Huang WS, Qi J, Thomas RM, Wang Y, Zhang S, Dodd R, Liu S, Xu R, Xu Y, Miret JJ, Rivera V, Clackson T, Shakespeare WC, Zhu X, Dalgarno DC. Fragment growing and linking lead to novel nanomolar lactate dehydrogenase inhibitors. Journal of medicinal chemistry. 2013; 56(3): 1023–40. [PubMed: 23302067]
29. DeLano, W. The PyMOL Molecular Graphics System. DeLano Scientific; San Carlos, CA: 2002. http://www.pymol.org/
30. Bell JK, Yennawar HP, Wright SK, Thompson JR, Viola RE, Banaszak LJ. Structural analyses of a malate dehydrogenase with a variable active site. J Biol Chem. 2001; 276(33):31156–62. [PubMed: 11389141]
31. Hall MD, Banaszak LJ. Crystal structure of a ternary complex of Escherichia coli malate dehydrogenase citrate and NAD at 1.9 A resolution. J Mol Biol. 1993; 232(1):213–22. [PubMed: 8331658]
32. Swiderek K, Panczakiewicz A, Bujacz A, Bujacz G, Paneth P. Modeling of isotope effects on binding oxamate to lactic dehydrogenase. J Phys Chem B. 2009; 113(38):12782–9. [PubMed: 19715328]
33. Kolappan S, Shen DL, Mosi R, Sun J, McEachern EJ, Vocadlo DJ, Craig L. Structures of lactate dehydrogenase A (LDHA) in apo ternary inhibitor-bound forms. Acta Crystallogr D Biol Crystallogr. 2015; 71(Pt 2):185–95. [PubMed: 25664730]
34. Pai EF, Schulz GE. The catalytic mechanism of glutathione reductase as derived from x-ray diffraction analyses of reaction intermediates. J Biol Chem. 1983; 258(3):1752–7. [PubMed: 6822532]
35. Cortes A, Cascante M, Cardenas ML, Cornish-Bowden A. Relationships between inhibition constants, inhibitor concentrations for 50% inhibition and types of inhibition: new ways of analysing data. The Biochemical journal. 2001; 357(Pt 1):263–8. [PubMed: 11415458]

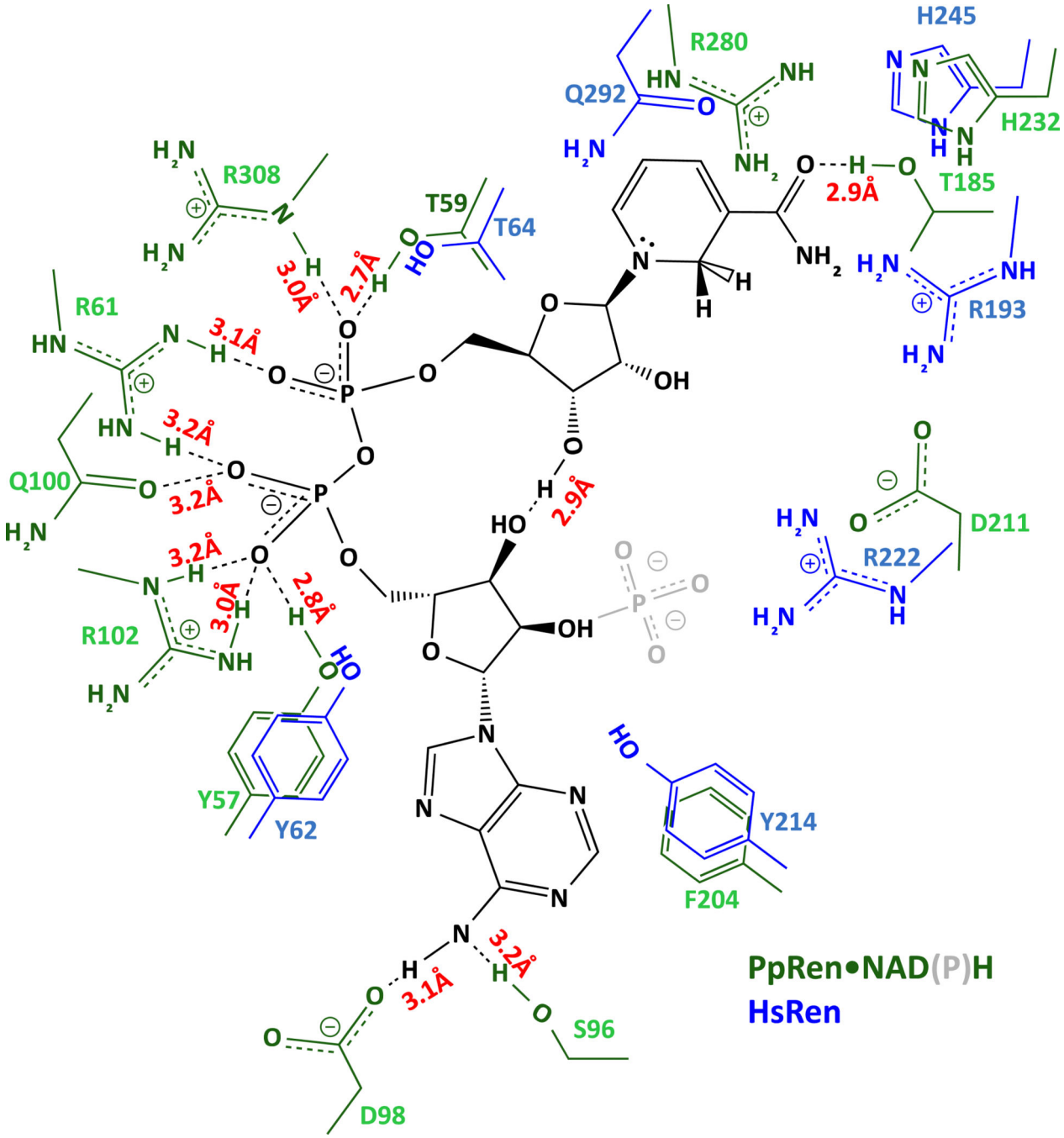

Figure 1. Two-Dimensional Representation of Active Site Interactions of NAD(P)H Molecules with Bacterial and Human Renalase

Structure in black is the NAD(P)H ligand; green indicates residues from *Pseudomonas phaseolicola*. Residues shown in blue are the conserved and non-conserved residues from human renalase that are proximal to the interacting residues from the *P. phaseolicola* structures. The 2'-phosphoryl of NADPH is shown in grey. Apparent hydrogen bond and charge interaction distances are shown in red

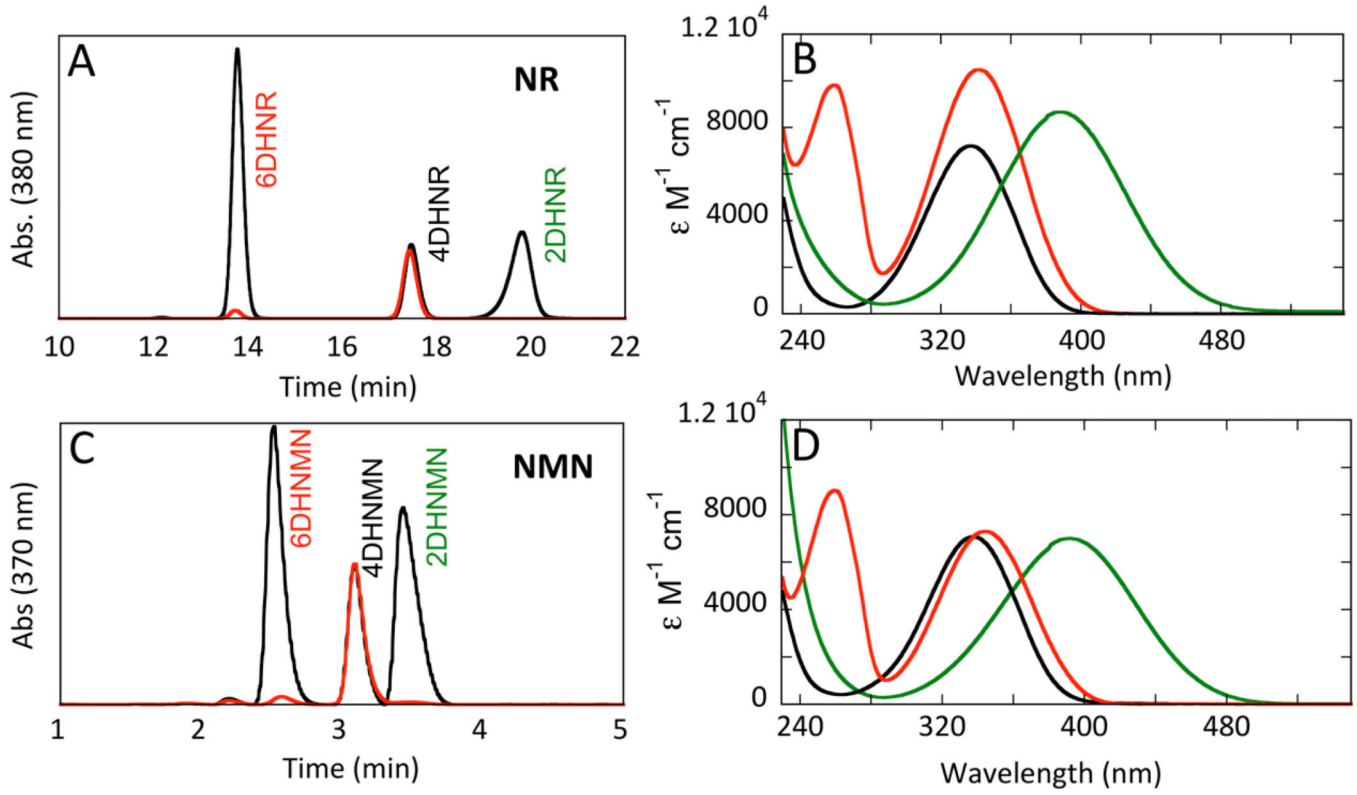

Figure 2. Oxidation of Dihydronicotinamide Nucleosides (NR) and Mononucleotide (NMN) Substrates by Renalase

NR^+ and NMN^+ were reduced by the addition of sodium borohydride forming three reduced isomers of each. These mixtures were then reacted with renalase (12.5 μM) for 10 minutes. A and C are HPLC chromatograms that showed the three species formed by reduction without (black trace) and with (red trace) the incubation with renalase. B and D are the extinction coefficient spectra for each of the reduced forms obtained, each corresponding to the chromatograms shown to the left.

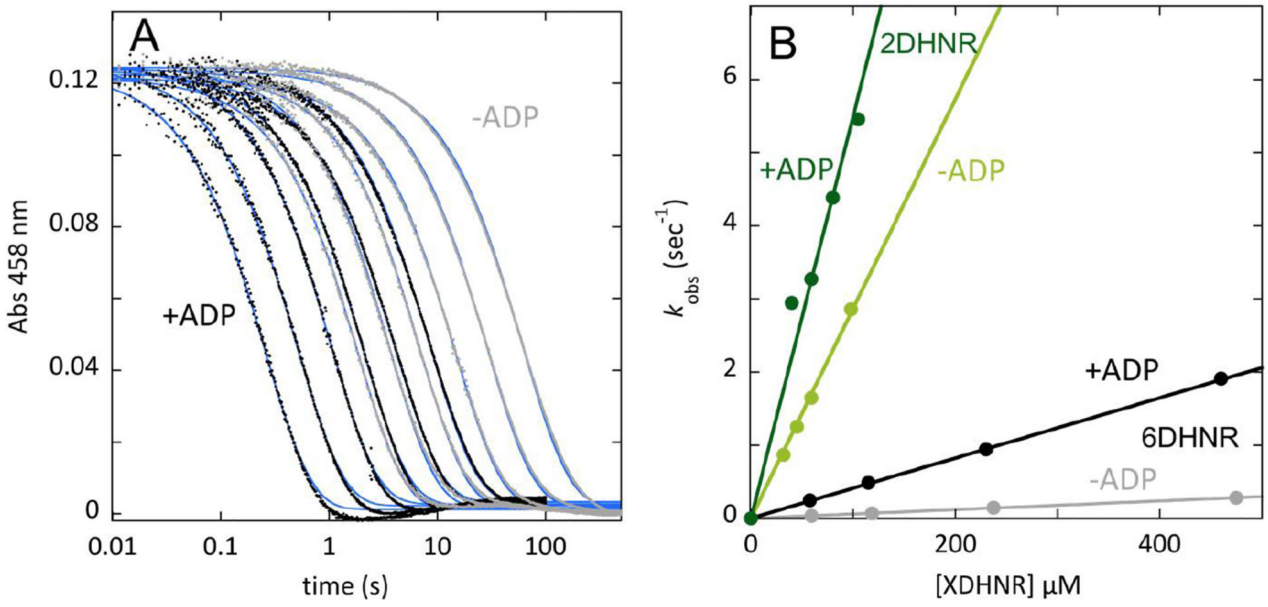

Substrate	Complimentary Ligand	k_{red}/K_d nM^{-1}/s^{-1} HsRen	Factor	k_{red}/K_d nM^{-1}/s^{-1} PpRen	Factor
6DHNMN	+AMP (1.12 mM)	30.0 ± 0.3		0.032 ± 0	
	-AMP	30 ± 1	1.0	0.063 ± 0.002	2.0
2DHNMN	AMP (1.12 mM)	160 ± 2		22 ± 1	
	-AMP	170 ± 4	1.1	26 ± 2	1.2
6DHNR	ADP (3.95 mM)	59 ± 0		0.039 ± 0.005	
	-ADP	4.1 ± 0	7.0	0.028 ± 0.004	0.7
2DHNR	ADP (4.83 mM)	29.0 ± 0.3		1.0 ± 0.1	
	-ADP	55 ± 3	1.9	0.55 ± 0.04	0.6

Figure 3. Reductive Half Reactions with 2- and 6Dihydro- NMN and NR with and without complementary ligands

A. Representative reduction traces for HsRen (10 µM) reacting with 6DHNR in the presence (black) and absence (grey) of 4 mM ADP. Data were fit to a single exponential according to equation 1. Lines of best fit over the data (blue). B. Secondary plot showing the effect of added ADP on the observed rate constant for reduction of HsRen by both 2- and 6DHNAD. Data were fit to equation 2 to determine values for K_{red}/K_d from the slope term.

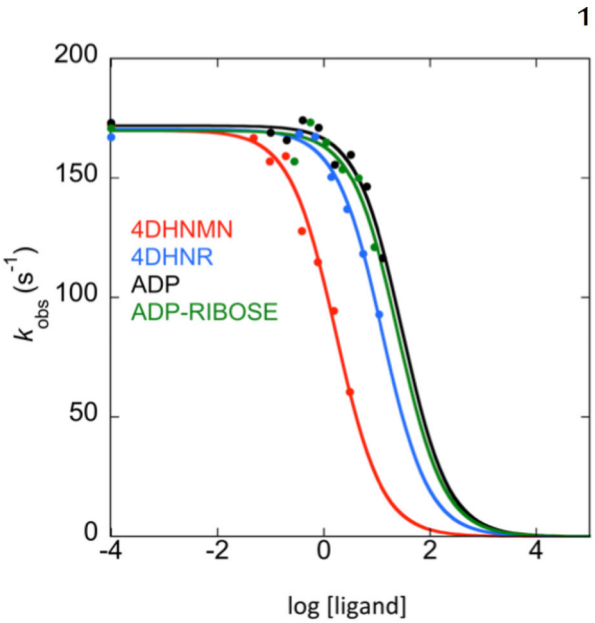

Ligand	K_d (mM)
ADP	15.0±0.6 [a]
ADP-ribose	12.4±0.5 [a]
NAD^+	2.8±0.3
4DHNR	6.1±0.5 [a]
4DHNMN	1.0±0.5 [a]
4DHNADP (NADPH)	1.5±0.4 [b]
4DHNAD (NADH)	0.6±0.1 [b]
6DHNAD	0.17±0.01 [b]
2DHNAD	0.17±0.01 [b]

a- Values estimated from suppression of the reduction rate constant obtained in the presence of 6DHNAD at a concentration equivalent to the K_d for that substrate (170 μM).

b- Values reproduced for reference from Beaupre et al., 2015[2].

Figure 4. Estimates of Binding constants for substrate fragments and substrate analogs with HsRen

The plot shows the partial IC_{50} curves used to estimate the binding constants of non-substrate ligands that exhibited inhibition. The fit of the curve to equation 3 gave IC_{50} values that by the methods used is twice the K_d (or K_i) for the inhibitory ligand [35]. No evidence of inhibition of the reductive half reaction was observed for AMP (7.6 mM), nicotinamide (68 mM), N-methyl-nicotinamide (7.8 mM), NR^+ (7.3) mM), NMN^+(2.6 mM) with values in parentheses indicating maximal concentration tested for evidence of inhibition.

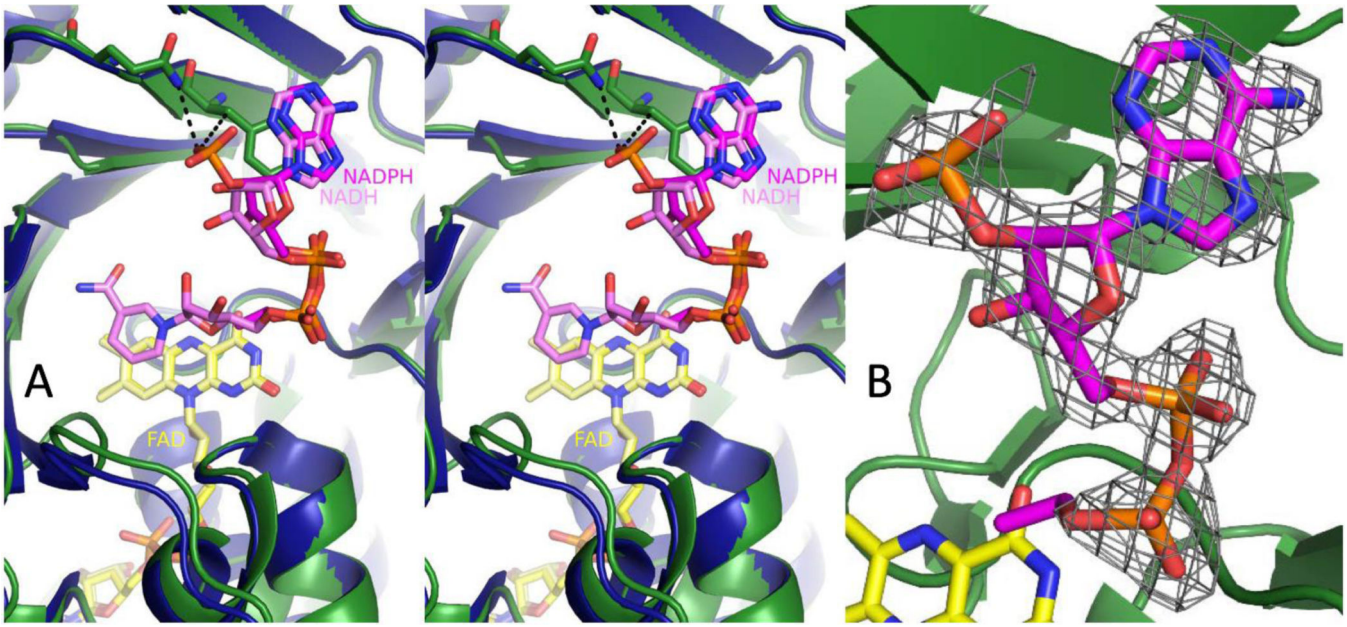

Figure 5. β-NADH vs β-NADPH Binding to PpRen

A. Stereo view of the β-NADH-renalase (PDB: 4ZCC, blue cartoon) overlaid on the NADPH-renalase (structure determined here, green cartoon). FAD is colored with carbon atoms yellow for both molecules. The β-NADH is shown with pink carbon atoms and the NADPH is magenta. The two most proximal residues are shown with carbon atoms green. The phe204 ring stacks with the adenine ring of β-NAD(P)H. The β-carbon of phe204 is 3.9 Å from one oxygen of the 2-phosphoryl group. The amide-nitrogen of gln206 is 3.4 Å from the same oxygen; however, the density is poor for this sidechain. Note that the FAD is buried, and that the β-NAD(P)H is bound to a cleft on the exterior of the protein. B. A simulated annealing omit map contoured at 3σ surrounds the β-NADPH (omitted in calculation) shows that the nicotinamide and nicotinamide-ribose of NADPH are not resolved in the map.

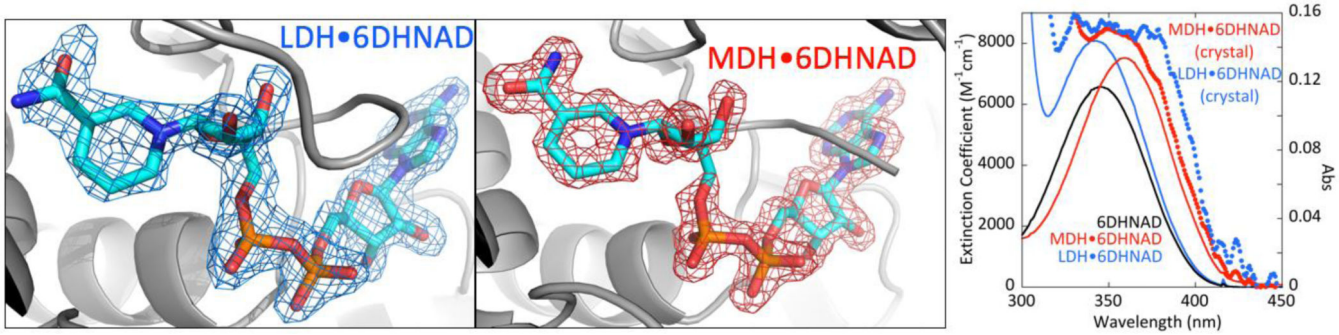

Figure 6. 6DHNAD inhibitory complex structures with MDH and LDH with 6DHNAD bound

Structural figures show that simulated annealing omit maps contoured at 3σ surround the 6DHNAD. **C. Absorption** Spectra recorded in solution (solid lines) and from the crystals used to solve the structures shown at left (dotted lines). These spectra show the presence of the 6DHNAD dihydronicotinamide chromophore in the crystals used to solve the structures.

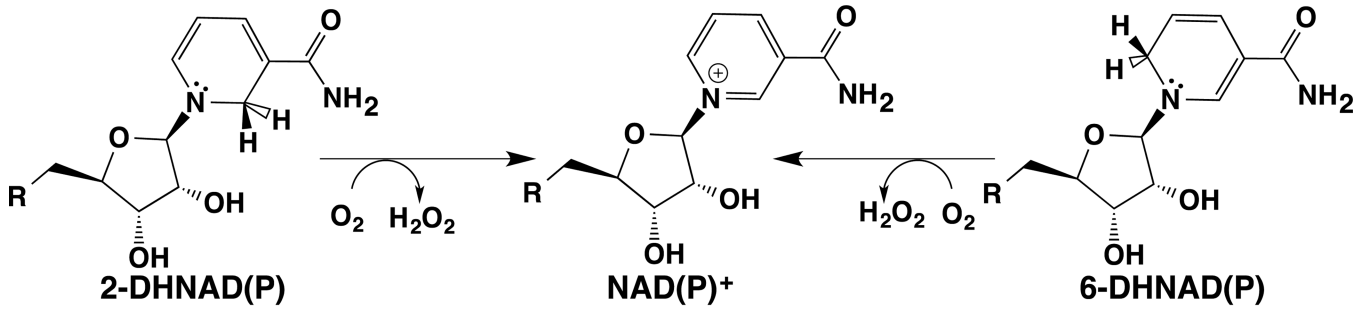

Nicotinamide mononucleotide (NMN) R = PO_4^{2-}
Nicotinamide riboside (NR) R = OH

Scheme 1.

Table 1

Structural Statistics for the MDH•6DHNAD, LDH•6DHNAD and PpRen•NADPH complexes

	MDH with 6DHNAD	LDH with 6DHNAD	PpRen with NADPH
Data collection[a]			
Beamline	9-2 (Stanford)	9-2 (Stanford)	21-ID-F (APS)
Wavelength (Å)	0.9795	0.9795	0.9787
Space group	$P2_12_12_1$	$P2_1$	$P2_1$
Cell dimensions; *a, b, c* (Å), β (°)	77.5, 83.8, 89.3, 90	63.6, 126.1, 84.2, 99.9	63.4, 71.0, 74.8, 107.8
Resolution range (Å)[b]	39.40 – 1.75 (1.78 – 1.75)	39.41 – 1.86 (1.89 – 1.86)	46.02 – 2.09 (2.16 – 2.09)
R_{merge}[c]	0.075 (0.548)	0.066 (0.574)	0.071 (0.357)
Total observations	286641 (14580)	373153 (16868)	119090 (10,650)
Total unique observations	58987 (3036)	108172 (5057)	37,538 (3,197)
Mean ($\langle I \rangle$ / σ(I))	14.3 (2.6)	11.8 (2.0)	11.2 (2.6)
Completeness (%)	99.2 (94.0)	98.7 (93.2)	98.0 (96.0)
Redundancy	4.9 (4.8)	3.4 (3.3)	3.2 (2.9)
Wilson B-factor (Å^2)	14.41	19.98	24.99
Refinement			
Resolution (Å)	38.76 – 1.75 (1.81 – 1.75)	39.41 – 1.86 (1.93 – 1.86)1.996)	46.02 – 2.09 (2.16 – 2.09)
R_{cryst}[d]	0.1545 (0.1915)	0.1698 (0.2762)	0.157 (0.196)
R_{free}	0.1809 (0.2173)	0.2104 (0.3050)	0.203 (0.287)
Total unique observations	58918 (5659)	107967 (10506)	37198 (3037)
No. of non-H atoms in model:			
Protein	4381	10053	4958
Ligand	88	245	172
Water	473	506	198
rms deviation bonds (Å)	0.010	0.012	0.012
rms deviation angles (°)	1.103	1.17	1.46
Overall mean B-factor (Å^2)	17.34	26.32	35.39
Ramachandran plot analysis[e]			
Favored region	99.0	97.4	98.0
Allowed region	1.0	2.6	2.0
Outlier region	0.0	0.0	0.0

[a] data indexed and scaled with XDS

[b] values in paretheses are for the highest resolution shell

[c] $R_{merge} = \Sigma_h|I_h - \langle I \rangle|/\Sigma_h I_h$, where I_h is the intensity of reflection h, and $\langle I \rangle$ is the mean intensity of all symmetry-related reflections

[d] $R_{cryst} = \Sigma||F_O| - |F_C||/\Sigma|F_O|$, F_O and F_C are observed and calculated structure factor amplitudes. Five percent of the reflections were reserved for the calculation of R_{free}.

[d] Calculated with Molprobity